IEEE Access
Multidisciplinary | Rapid Review | Open Access Journal

Received 26 October 2022, accepted 6 December 2022, date of publication 15 December 2022, date of current version 21 December 2022.

Digital Object Identifier 10.1109/ACCESS.2022.3229388

RESEARCH ARTICLE

A Cooperative Method Based on Joint Electric and Magnetic Cleanliness for Space Platforms EMC Assessments

NIKOLAOS FRAGIADAKIS, ANARGYROS T. BAKLEZOS, THEODOROS N. KAPETANAKIS, IOANNIS O. VARDIAMBASIS, AND CHRISTOS D. NIKOLOPOULOS

Department of Electronic Engineering, School of Engineering, Hellenic Mediterranean University, 73133 Chania, Greece

Corresponding author: Christos D. Nikolopoulos (cnikolo@hmu.gr)

This work was supported in part by the project "Strengthening and Optimizing the Operation of Financial and Administrative Support Unit (MODY) Services and Academic and Research Units of the Hellenic Mediterranean University," and in part by the Public Investment Program of the Greek Ministry of Education and Religious Affairs.

ABSTRACT A lot of studies for spacecraft design have been carried out in the past to ensure space mission success without compromising the scientific data but electromagnetic issues always puzzle engineers. The mission science objectives rely on the scientific payload high sensitivity to accurately capture the space environment. Electromagnetic cleanliness is a permanent issue in order for the measurements to reflect that and not the spacecraft emissions. The majority of the past and current ESA's, NASA's and JAXA's science missions utilizes more or less the same basic working units, i.e. RF switches, batteries, Command & Data Handling Management units, Power Conditioning and Distribution Units, S-Band Transceivers, etc. These components that can be easily measured and electromagnetically characterized in ground facilities and testing laboratories. This work provides the framework for a complete unit positioning methodology, considering the unit test-level information, in order to predict and properly allocate the spacecraft equipment for simultaneous electric and magnetic cleanliness even in different sensors locations. This methodology can be adapted for a fast pre-compliance testing and possibly early design considerations in every space mission.

INDEX TERMS Differential evolution, electromagnetic cleanliness, inverse electromagnetic problem, spacecraft unit allocation.

I. INTRODUCTION

Space equipment by definition is, in the majority, complex electronic systems that are very sensitive to electromagnetic compatibility (EMC) issues, demanding rigorous testing and harsh cleanliness requirements [1], [2], [3]. Characterization and modeling of the radiated emissions, both electric and magnetic, from any device or harness on board satellites is mandatory to the design phase in order to prevent EMI/EMC issues at system level [4], [5]. The units are characterized with respect to their electromagnetic emissions in order to enable the on-ground scientific and technical crew to assemble a platform unit arrangement with acceptable, per the specific mission requirements, field emissions at the various sensitive sensor locations. Moreover, common practice includes the modelling of said equipment, at unit level, in order to be able to extrapolate the produced fields at the intended sensor locations for an initial, best engineering guess, placement of each unit.

Of course, this usually leads to emitted fields well over the technical and scientific mission requirements. The usual treatment for these issues is to relocate units with significant emissions as far as possible from the selected sensor locations [6]. Of course, this remedy has a limited field of application since the available space in the platform is finite. So, booms were introduced to further separate sensors and other units, however missions get more and more complex carrying an increasing number of units and on of that the requirements get increasingly stringent with time.

The associate editor coordinating the review of this manuscript and approving it for publication was Mehmet Alper Uslu.

More advanced techniques have been applied for these kind of issues such as the (passive) shielding [7], [8] of either specific subcomponents [7] or whole equipment units, e.g. reaction wheels [8], which cause issues with their emissions. Commonly used materials, appropriate for this task, are Mu-metal or Metglass [6], [9]. The shielding is a solution that inadvertently adds to the total mass of the platform and can only be applied to certain units in order to not hinder their operation.

An even more complex technique is the active mitigation/cancelling of the emitted fields [7], [10], [11] via the use of additional specially selected ''artificial'' sources with careful placement in the platform in order to produce opposite fields which actively cancel either the field of a selected unit [7], [10], or the total field of the platform at selected locations or regions of interest, where the most sensitive sensors or equipment are placed, enabling the system level emissions to comply with the mission requirements. This technique spans from solutions like compensation magnets [6], [7] for DC issues to low frequency active system [10], [11].

This frequency diversification highlights another critical aspect of the cleanliness subject; the frequency range of operation of the various mission specific sensors. These ranges set the mission cleanliness requirements which in turn decide the range of the necessary characterization of units and the actual remedies to be applied in case of problems. Direct current (DC) issues are well known and there are guidelines [12] in place to help prevent or minimize them at the design phase of the mission. These include avoiding ''hard'' magnetic materials, reducing current loop area [13], Solar Panel backwiring [14], etc., for the DC magnetic field. The electrostatic problem plays also a major role in the system design. Surface charging alters the electrostatic environment of the platform so the differential potential of any pair of points of the surface of the spacecraft surface is also required to be at a minimum (commonly below 1 V). For this to happen all spacecraft surfaces need to be highly conducting [15]. On the other hand, the low frequency alternating current (AC) cleanliness issues however are a relatively new domain which attracts increasing attention [9], [10], [11], [13].

As stated, a complete system level EMC campaign needs to meet strict cleanliness requirements. It has to include both electric and magnetic fields, from any device or harness onboard the mission platform. In this work, author propose a joint electric and magnetic cooperative methodology for DC and low frequencies, in order to minimize both electric and magnetic fields at the sensors' distinct location. This is done by rearranging the onboard units, position as well as orientation. These field minimization problems have been addressed separately by the authors in the past [16], [17]. However, in missions' more often than not, there are instruments measuring both fields. In those cases, a placement fit to minimize the electric field at a desired location (electric sensor) might maximize the magnetic field at another desired location (magnetic sensor). This work provides a joint cooperative methodology and showcases that simultaneous solution for both problems is feasible. It should be noted that the proposed methodology takes into consideration the emissions of only units and omits emissions from cables and harnesses.

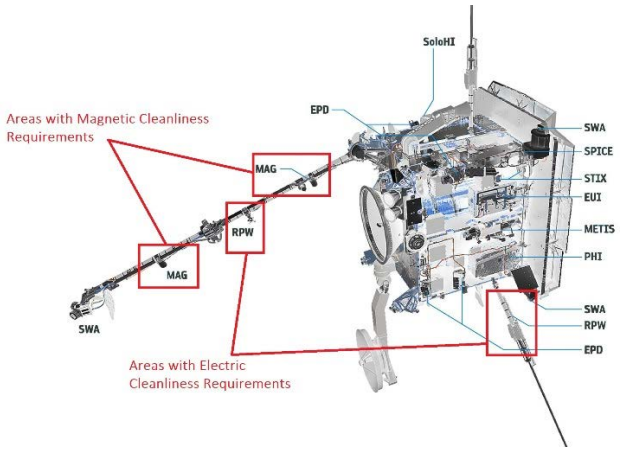

FIGURE 1. Sensor's accommodation on Solar Orbiter boom. Credit: ESA – Areas with Electric & Magnetic Cleanliness Requirements.

The system level radiated emission prediction from unit level measurements does not only simplify the test methodology and decrease the total EMC campaign costs but can also provide a pathway to achieve a desired electromagnetic cleanliness to a specific location by proper allocation of the space platform equipment [16], [17].

The rest of the paper is structured as follows, Section II discusses briefly the cleanliness problem's mathematical formulation and modeling methodology regarding emissions estimation both for the electric and magnetic field. Section III presents the simulation results on an actual cleanliness scenario for both the magnetic and electric field sensors on their original placement on the Solar Orbiter's boom. Finally, the paper is concluding on section IV with future research guidelines.

II. BRIEF MATHEMATICAL BACKGROUND & PROBLEM FORMULATION DISCUSSION

The essence of electromagnetic cleanliness is the minimization of the electromagnetic emissions at a location of interest, where various sensitive equipment or sensors are meant to be placed. In the unit level modeling process, each unit has its electromagnetic behavior characterized and attributed to typical equivalent sources (e.g. dipoles) in order to enable the prediction of the unit field emissions everywhere in space and for various modes of operation. Then, the system level behavior is estimated by the vectorial summation of the emissions of all the units, or at least the ones who are identified as the major contributors, at the region of interest.

A. ELECTRIC AND MAGNETIC FIELD FORMULATION

The frequency range of interest, in the present work, spans from DC to the low frequencies ($f < 300$ kHz). In this range,

and especially close to the source of the field (distances much less than a wavelength) the problem of the calculation of the field emitted from the source is considered quasistatic so each field, electric and magnetic, is treated independently of the other. For this specific set of conditions (low frequencies, area of interest close to the unit-sources) a near field approximation is justified. The core representation for the electric/magnetic behavior of each unit is an electric/magnetic dipole for each frequency of interest. An approach with more dipoles per unit is possible and the analysis presented fully supports it, however since it is not common practice, it will not be addressed specifically in this work. In any case, each such dipole for each frequency is represented with its corresponding moment and position, inside the unit space, variables.

Expressing the position vector of a dipole source as $\boldsymbol{R}_{dipole}$, the moment vector of the dipole as $\boldsymbol{p}$ and as $\boldsymbol{R}_m$ the position vector of an observation point K, utilizing the near field approximation the electric and magnetic fields are expressed as:

$$\boldsymbol{G}(\boldsymbol{n}, t) = Ae^{-i\omega t}\{3\boldsymbol{n}(\boldsymbol{n}\cdot\boldsymbol{p}) - \boldsymbol{p}\}\frac{1}{r^3} \tag{1}$$

For the electric field, $\mathrm{A} = \frac{1}{4\pi\varepsilon_0}$ and $\boldsymbol{p}$ is the electric dipole moment vector, while for the magnetic field, $A = \frac{\mu_0}{4\pi}$ and $\boldsymbol{p}$ is the magnetic dipole moment vector. Moreover, $\boldsymbol{r} = \boldsymbol{R}_m - \boldsymbol{R}_{dipole}$, $r = |\boldsymbol{r}|$ and $\boldsymbol{n} = \frac{\boldsymbol{r}}{r}$.

In accordance with this formulation, and for each frequency of notable emissions, $\omega_i = 2\pi f_i$, each field $\boldsymbol{G}$ at K with $\boldsymbol{R}_m$ (x_m, y_m, z_m), can be analyzed to the three components:

$$\left.\begin{aligned} G_x &= A\left[\frac{3(x_m-x)\cdot C}{r^5} - \frac{p_x}{r^3}\right] \\ G_y &= A\left[\frac{3(y_m-y)\cdot C}{r^5} - \frac{p_y}{r^3}\right] \\ G_z &= A\left[\frac{3(z_m-z)\cdot C}{r^5} - \frac{p_z}{r^3}\right] \end{aligned}\right\} \tag{2}$$

where:

$$C = p_x\cdot(x_m - x) + p_y\cdot(y_m - y) + p_z\cdot(z_m - z)$$

and

$$r = \sqrt{(x_m-x)^2 + (y_m-y)^2 + (z_m-z)}^{\,2}.$$

So, for the angular frequency ω_i the total magnitude of the field from a single dipole is:

$$|\boldsymbol{G}_{total}|_i = \sqrt{G_x^2 + G_y^2 + G_z^2} \tag{3}$$

Considering N un its are contributing to the system emissions, therefore N different dipoles or N dipoles corresponding to Q units (N>Q, hence more than one dipole per unit, the total field components at a measurement point *m,* are:

$$G_{Total\,s} = \sum_{i=1}^{N} A\left[\frac{3\,(s_m - s_i)\cdot C}{r^5} - \frac{p_{si}}{r^3}\right] \tag{4}$$

where s: x, y, z expressing the corresponding component and the total amplitude for either electric or magnetic field is:

$$|\boldsymbol{G}_{total}|_N = \sqrt{G_{xTotal}^2 + G_{yTotal}^2 + G_{zTotal}^2} \tag{5}$$

B. SYSTEM MODEL ASSEMBLY FOR THE ESTIMATION OF SYSTEM EMISSIONS

In order to perform the calculations of (2) and summations of (3) and (4) the variables of the dipoles (location and moment components) must be expressed in a common coordinate system. This is commonly selected to be the Spacecraft Coordinate System (SCS). In the SCS, which refers to the actual placement of the units in the spacecraft system, each unit can be rotated along the 3 axes as well as be moved around in the 3-dimentional space, naturally within the spacecraft bounds.

Let's consider the j-th equipment unit (DUT) with its center at (x_{oj}, y_{oj}, z_{oj}) considering the Spacecraft origin (Spacecraft's Coordinate System - SCS), with all the parameters reflected in Fig.3. Every equipment unit is represented by k dipoles, with $k < i$. For the calculation of the orientation of the corresponding moment vector (both for the electric and the magnetic) in case where the DUT is rotated in all directions (where θ, ω *and* φ the corresponding orientation angles on the three-axial system) the transformation matrices depicted below (6) should be employed:

$$\left.\begin{aligned} R_x &= \begin{bmatrix} 1 & 0 & 0 \\ 0 & cos\theta & -sin\theta \\ 0 & sin\theta & cos\theta \end{bmatrix} \\ R_y &= \begin{bmatrix} cos\omega & 0 & sin\omega \\ 0 & 1 & 0 \\ -sin\omega & 0 & cos\omega \end{bmatrix} \\ R_z &= \begin{bmatrix} cos\varphi & -sin\varphi & 0 \\ sin\varphi & cos\varphi & 0 \\ 0 & 0 & 1 \end{bmatrix} \end{aligned}\right\} \tag{6}$$

resulting to the following effect on the moments and spatial coordinates:

$$\begin{pmatrix} p_{x_{kj}} \\ p_{y_{kj}} \\ p_{z_{kj}} \end{pmatrix}_{(rotated)} = R_z R_y R_x \begin{pmatrix} p_{x_{kj}} \\ p_{y_{kj}} \\ p_{z_{kj}} \end{pmatrix}_{(initial)} \tag{7}$$

$$\begin{pmatrix} x_{o_{kj}} \\ y_{o_{kj}} \\ z_{o_{kj}} \end{pmatrix}_{(rotated)} = R_z R_y R_x \begin{pmatrix} x_{o_{kj}} \\ y_{o_{kj}} \\ z_{o_{kj}} \end{pmatrix}_{(initial)} \tag{8}$$

The order on the rotation execution to the center of the DUT is always initially on the x-axis, then on y-axis, and lastly on the z-axis. It should be noted that the coordinates

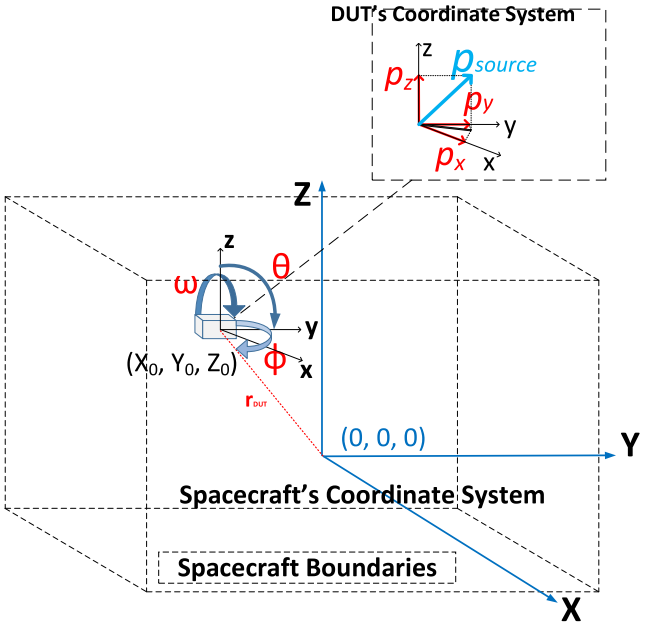

FIGURE 2. Coordinate system transformation - DCS to SCS.

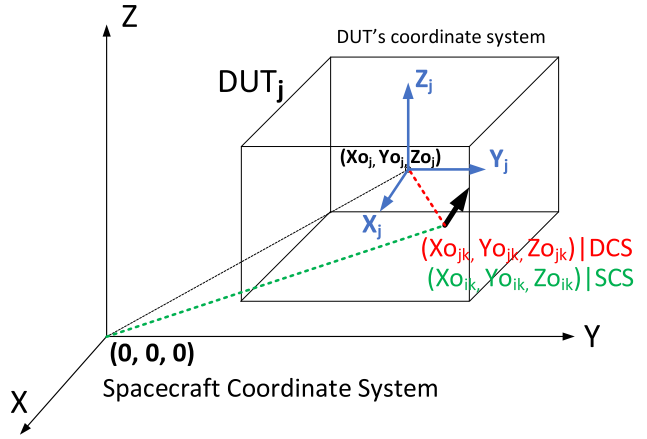

FIGURE 3. Coordinate system transformation - DCS to SCS.

and the moment vectors of the dipole source are calculated from the (7) and (8).

The $k-th$ dipole is placed at $(x_{okj}, y_{okj}, z_{okj})$ with reference to the j-th equipment unit's origin (Device Coordinate System - DCS) and, and for the calculation of the total electric/ magnetic field (according to (4) and (5)), the dipoles' coordinates (at DCS, $x_{oij}, y_{oij} z_{oij}$) should be transformed to the SCS coordinate system by:

$$\left.\begin{aligned} x_{oij} &= x_{okj}, +x_{oj} \\ y_{oij} &= y_{okj} + y_{oj} \\ z_{oij} &= x_{okj} + z_{oj} \end{aligned}\right\} \tag{9}$$

This way for any displacement and possible rotation, applying (9) and (7) respectively, the orientation of the center of the DUT and the moment vector (electric and/ or magnetic) are expressed in SCS.

TABLE 1. DUT's electric moments.

DUT/Dipoles	p_x (fC · m)	p_y (fC · m)	p_z (fC · m)
1	3	12	4
2	8	-9	25
3	7	-5	13
4	-23	-1	6

TABLE 2. DUT's magnetic moments.

DUT/Dipoles	m_x (mA · m^2)	m_y (mA · m^2)	m_z (mA · m^2)
1	-0.9	-27	-41
2	4.1	-90	94
3	-3.6	-53	1.6
4	-23	9.3	11

TABLE 3. DUT's dimensions.

DUT	L(m)	W(m)	H(m)	R_i(m)
1	0.4	0.4	0.2	0.3
2	0.2	0.25	0.3	0.2194
3	0.4	0.1	0.1	0.2121
4	0.3	0.3	0.2	0.2345

C. PROBLEM DEFINITION

In every space mission, numerous DUTs exist on board bounded from the spacecraft's hull. This way in our case, the spacecraft container has been simulated with a cuboid volume with dimensions 2.5 m × 2.5 m × 3 m (Fig. 2). This volume consists also the bounding area for all the units' displacement. It should be noted, as mentioned in the introduction section, various actual equipment units (DUTs) from Gravity Field and Steady-State Ocean Circulation Explorer (GOCE) mission were measured and modeled as presented in [18], providing a baseline for the electric and magnetic moments for the equipment units under test (artificial DUTs) of this paper, aimed to showcase the practical aspects of this endeavor.

In ordinary missions, the full spacecraft platform is comprised of various equipment units and instruments. T he integration of these devices forms the exact electromagnetic environment. However, usually only three or maybe four of them have an immense contribution and define the electromagnetic behavior/ signature of the system. Others are either discarded at the design phase or mass-modelled with a fixed moment value [19].

The four DUTs employed in this study, are considered operating at a single identical frequency, and each is modelled with one equivalent dipole assigned per unit, located at each center. The corresponding electric moments per DUT are tabulated in Table 1. The same modeling is used for the magnetic behavior of the units. The corresponding magnetic moments are tabulated in Table 2. The DUTs can be placed freely inside the container of the spacecraft boundaries.

The proposed methodology can also be applied in the case the DUT models consist of multiple electric/magnetic

dipoles, in order to include a more detailed modelling or to account for the induced electric/magnetic moment that is also usually modeled with an additional dipole [3], [20], [21],

The position where the measurement sensor or any other victim device, subject to the spacecraft emissions, needs to be placed, is the observation volume where electromagnetic cleanliness needs to be achieved. The sensor volumes, in this work, are considered cubes in shape, both with an edge of 0.2 m. The electric and magnetic sensors are referred to by their center (OP_e = 3.318 m, 0 m, 0.75 m), (OP_m = 5.386 m, 0 m, 0 m) in the SCS. The exact shape of the observation volume can be adapted to accommodate different cases. The specific setup is depicted in Fig. 1. In this work, a constraint has been imposed on the allowed orientation of the DUTs. The DUT's shall always have a face parallel to the spacecraft's bottom surface. This is due to the need to be able to mount the DUTs somehow either to spacecraft walls or other internal surfaces. This constraint, is expressed with the angles θ and ω being discretized ($\theta, \omega : \in \{0^0, 90^0, 180^0, 270^0\}$) while units are allowed to rotate freely only in z-axis ($0 \leq \varphi < 360$).

The orientation and the relative placement of the DUTs to the sensor location can significantly modify the observable electric and magnetic field at the sensor location, assuming a defined set of DUTs (modelled as magnetic and electric moments). Equations (2) and (3) can attest to that. To eliminate the electric and magnetic fields emitted by the DUTs at the sensor locations, their placement and orientation need to be carefully selected.

D. ALGORITHM DESCRIPTION: HEURISTIC MINIMIZATION OF THE FIELD

The purpose of this methodology is to provide a cooperative systematic approach able to synthesize an appropriate electromagnetic environment; minimizing the fields jointly at predefined volumes manipulating appropriately the placement and orientation of the magnetic and electric sources. The selected volume (sensor) is distinct for the electric and the magnetic field as indicated by the coordinates of their respective cube centers.

The proposed stochastic method tries to optimally address the question of rearranging the four units (DUTs' magnetic and electric dipole sources) and their orientation in order to cancel both the electric and magnetic fields at the sensors' volumes (centered at OP_e and OP_m) effectively providing electromagnetic cleanliness. In this work the well-known algorithm, in computational optimization, Differential Evolution (DE) [22] is utilized to provide the solution. The solution is the set of the Cartesian coordinates of the centers of the four DUTs in SCS and the corresponding rotation angles; a total of 24 variables for the 4 DUTs. The flowchart of the proposed methodology is depicted in Fig. 4.

DE is used to computationally optimize a problem (maximization or minimization of an objective or fitness function). In general, this function expresses the laws governing the problem or a necessary condition. More specifically, it is a mathematical expression of the desired outcome of the process. In this scenario, the solution should minimize both the

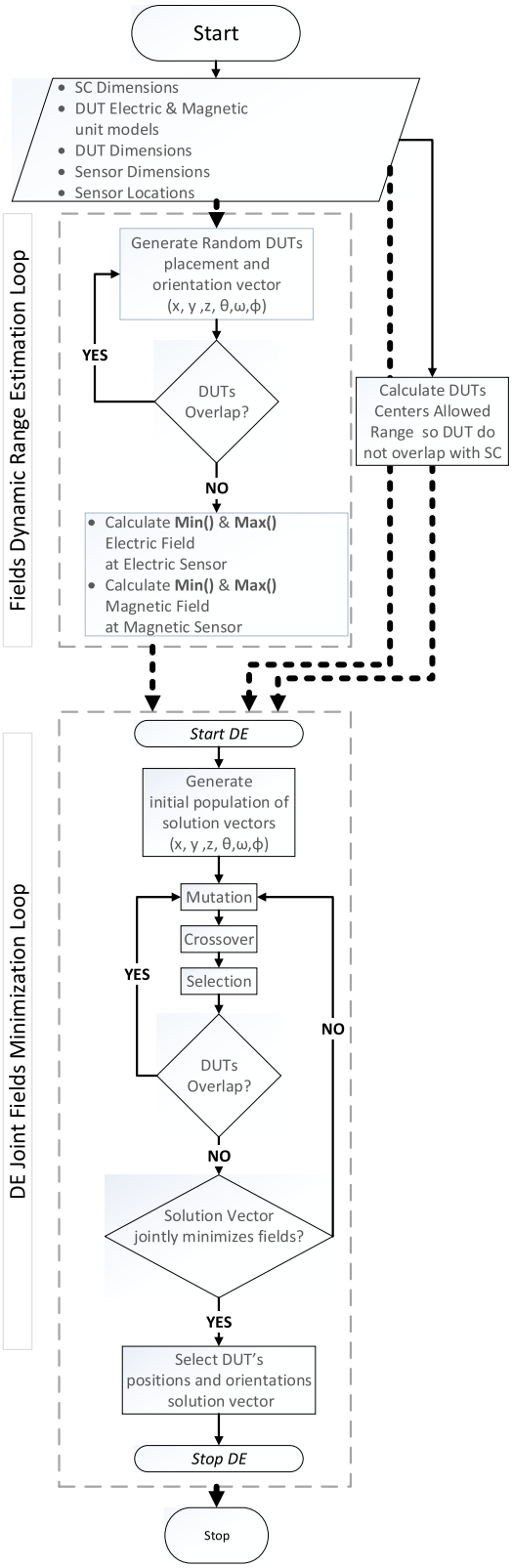

FIGURE 4. Algorithm flowchart for the DUTs arrangement for joint electric and magnetic field minimization.

electric $|\boldsymbol{E}|_t$ and the magnetic $|\boldsymbol{B}|_t$ field at their corresponding locations of interest $(\mathrm{OP_e}, \mathrm{OP_m})$. So, the fitness or objective function O could be formulated as:

$$\mathrm{O} = \frac{\mathbf{1}}{\mathbf{2}} \cdot |\mathbf{E}|_{\mathbf{t}} + \frac{\mathbf{1}}{\mathbf{2}} \cdot |\mathbf{B}|_t \tag{10}$$

This expression for the objective function should provide equal weights to the electric and magnetic field minimization, however in practice since the electric field has generally larger values (in absolute numbers) than the magnetic field at their respective sensor positions, it heavily leans towards the minimization of the electric field and is rather insensitive to the changes of the magnetic field due to the direct summation of their values.

To correct this issue and provide equal weights the field expressions need to be normalized taking into account the dynamic ranges of the fields for the specific set of units. For this reason, the objective function is rewritten as:

$$\mathrm{O} = \frac{\mathbf{1}}{\mathbf{2}} \cdot \frac{|\mathbf{E}|_t - \left|\tilde{\mathbf{E}}\right|_{\mathbf{min}}}{\left|\tilde{\mathbf{E}}\right|_{\mathbf{max}} - \left|\tilde{\mathbf{E}}\right|_{\mathbf{min}}} + \frac{\mathbf{1}}{\mathbf{2}} \cdot \frac{|\mathbf{B}|_t - \left|\tilde{\mathbf{E}}\right|_{\mathbf{min}}}{\left|\tilde{\mathbf{E}}\right|_{\mathbf{max}} - \left|\tilde{\mathbf{E}}\right|_{\mathbf{min}}} \tag{11}$$

where $\left|\tilde{E}\right|$ and $\left|\tilde{B}\right|$ denote estimated values of the fields, acquired from simulations for random assortments of the units. The larger the number of such random assortments tested, the more accurate the minimum and maximum values of the fields used for the objective function and in return the better the normalization achieved.

This way the objective function minimizes both fields with equal weights. However, given that the sensors are not considered as points but expressed with cubic shapes, the electric and magnetic fields need to be minimized across the whole sensor cubes, so the objective function is further modified toexpress the sum of the amplitude of the electric/magnetic fields at the sensor volume boundaries which are delimited by the 8 corresponding cube peaks. Thus, the individual terms of (10) are set to:

$$|\mathbf{E}|_{\mathbf{t}} = \sum_{i=1}^{8} |\boldsymbol{E_N}|_i \tag{12}$$

$$|\boldsymbol{B}|_{\mathbf{t}} = \sum_{i=1}^{8} |\boldsymbol{B_N}|_t \tag{13}$$

where E_N and B_N are the total electric and magnetic field of the N dipoles of the units (N=4 in this work) at peak i (out of 8) of each sensor cube. In order for $|\mathbf{E}|_{\mathbf{t}}$ and $|\mathbf{B}|_{\mathbf{t}}$ to minimize (and in return O to minimize), the amplitude of each field registered at each peak (i) must also be minimized.

So, the minimization of O yields the best tradeoff in order for both sensor volumes to be found in the lowest possible respective fields.

The minimization algorithm starts with the initialization of the solution population. These are randomly drawn, according to the uniform distribution, from the valid 24-Dimensional solution space. The search space in this work

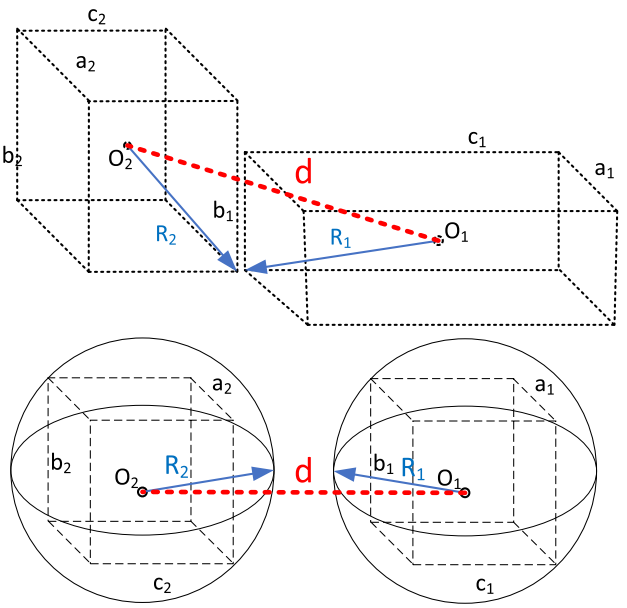

FIGURE 5. DUTs/ Circumscribed spheres placement constraint to avoid overlap.

is composed of the six variables of each DUT (four DUTs); the three coordinates of the center of each DUT (x_i, y_i, z_i) and the three rotation angles $(0 \leq \varphi \leq 360^0, \theta, \omega : 0^0, 90^0, 180^0, 270^0)$. The valid range for the center coordinates of each DUT will be discussed shortly. Next, the algorithm iteratively attempts to improve a candidate solution employing operations as mutation, crossover and selection, in order to minimize the objective function.

Following the generation of each prospect solution, its feasibility is initially evaluated with regard to DUT collision. It should be noted that this evaluation is also carried out for the solutions of the initial population but the step is omitted in the algorithm flowchart (Fig.4). The evaluation is executed by expressing a cuboid DUT with dimension a_i, b_i and c_i with its circumscribed sphere. The circumscribed sphere has a radius R_i:

$$R_i = \sqrt{\left(\frac{a_i}{2}\right)^2 + \left(\frac{b_i}{2}\right)^2 + \left(\frac{c_i}{2}\right)^2} \tag{14}$$

To avoid overlap, the two DUTs need to comply to:

$$d \geq R_1 + R_2 \tag{15}$$

where d is the center-to-center distance of the DUTs and R_1, R_2 the radii of the respective circumscribed spheres (Fig. 5).

In case the unit overlap condition is not met, the prospect solution is erased and replaced by a newly generated one, as depicted in the algorithm's flowchart in Fig. 4. This is done to further investigate only physically feasible solutions.

Moreover, each generated prospect solution shall not collide with the spacecraft boundaries. The prospect solution must yield DUT centers that lie at distances greater than R_i

TABLE 4. DUT center coordinates ranges.

Variable	Minimum Allowed Value	Maximum Allowed Value
x_1(m)	-0.95	0.95
y_1(m)	-0.95	0.95
z_1(m)	-1.2	1.2
x_2(m)	-1.0306	1.0306
y_2(m)	-1.0306	1.0306
z_2(m)	-1.2806	1.2806
x_3(m)	-1.0379	1.0379
y_3(m)	-1.0379	1.0379
z_3(m)	-1.2879	1.2879
x_4(m)	-1.0155	1.0155
y_4(m)	-1.0155	1.0155
z_4(m)	-1.2655	1.2655

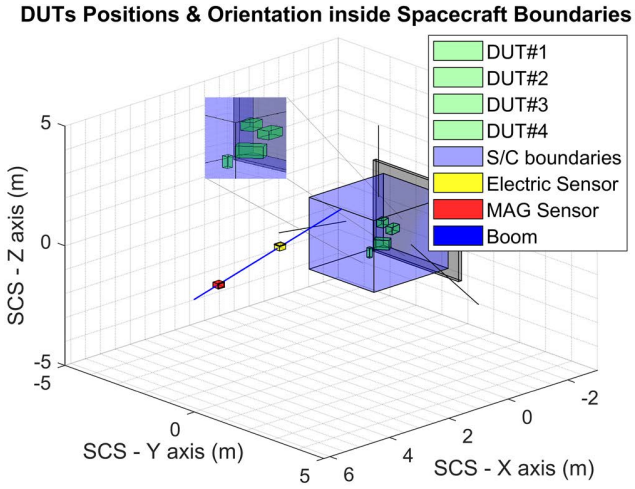

FIGURE 6. Non-overlapping DUTs in the spacecraft according to the algorithm solution and sensors on the boom.

TABLE 5. DUTs optimized variables (center position & orientation).

DUT	X (m)	Y (m)	Z (m)	θ	ω	φ
1	-0.95	-0.95	-1.2	90^0	180^0	125.1^0
2	-1.0306	-1.0306	-0.375	0^0	180^0	107.8^0
3	-0.396	-0.803	-1.2879	180^0	270^0	89^0
4	-0.846	-0.431	-0.338	90^0	90^0	10.4^0

from the spacecraft boundaries. This restriction yields the min/max values of the search space for the units' center coordinates tabulated in Table 4.

This criterion is obviously always satisfied since the corresponding variables cannot take values outside the allowed range. As discussed, it is relatively easy to enforce additional rules e.g., forbidden areas for certain units, and specific relative orientations or distances between selected unit pairs or unit-boundary pairs, etc.

The methodology fully supports such rules and expressions in order to formulate a specific problem.

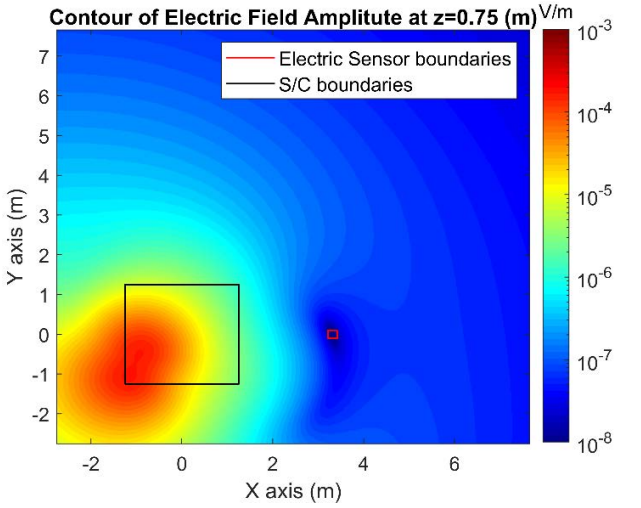

FIGURE 7. Electric field amplitude across the XY plane at the center of the electric sensor ($3.318\ m, 0\ m, 0.75\ m$).

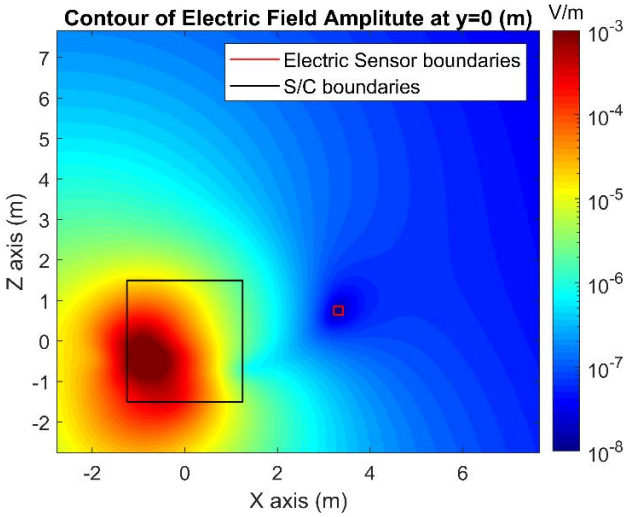

FIGURE 8. Electric field amplitude across the XZ plane at the center of the electric sensor ($3.318\ m, 0\ m, 0.75\ m$).

III. SIMULATION RESULTS AND DISCUSSION

Algorithm execution results are tabulated in Table 5 and depicted in Fig. 6. There is clearly no overlap between the DUTs and the specific assortment of DUTs leads to electric field amplitude equal to 2.57e-09 (V/m) and magnetic field amplitude 3.12e-14 (T) at the center of the corresponding sensor volume. The sensors (electric highlighted in yellow, magnetic highlighted in red) and the boom (highlighted in blue) are also depicted in Fig. 5.

Figures 7-9 depict contours of the electric field amplitude at the center of the electric sensor (3.318m, 0m, 0.75m). It is clear from Figs. 7-9 that the algorithm manages to rearrange the DUTs in such a way that the electric sensor is placed at the location of minimum electric field for each plane. Figures 7-8 are 3D slices of the electric field amplitude which cut through

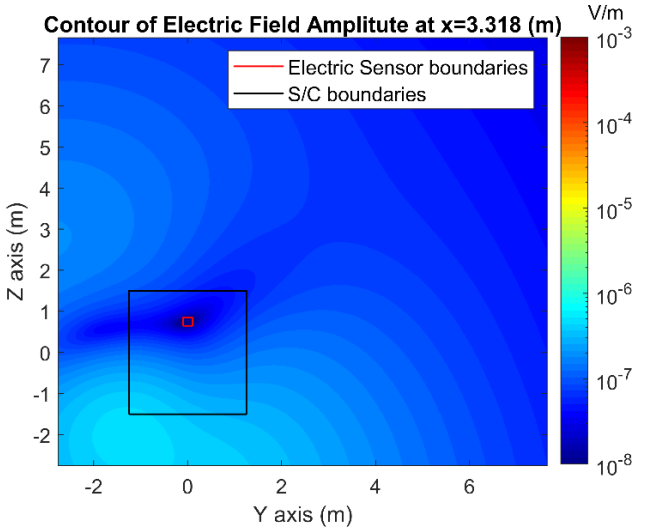

FIGURE 9. Electric field amplitude across the YZ plane at the center of the electric sensor ($3.318\ m$,$0\ m$,$0.75\ m$).

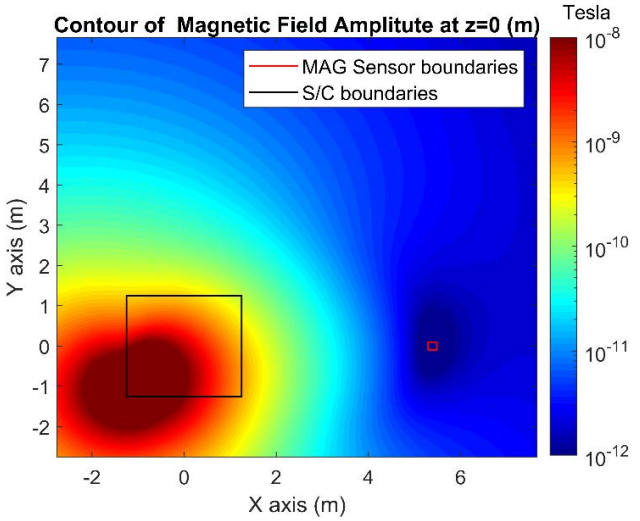

FIGURE 11. Magnetic field amplitude across the XY plane at the center of the magnetic sensor ($5.386\ m$,$0\ m$,$0\ m$).

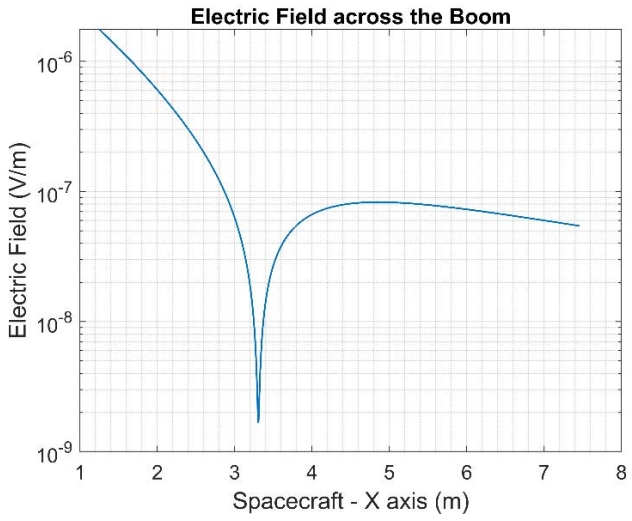

FIGURE 10. Electric Field amplitude on the boom. Minimum is at the electric sensor.

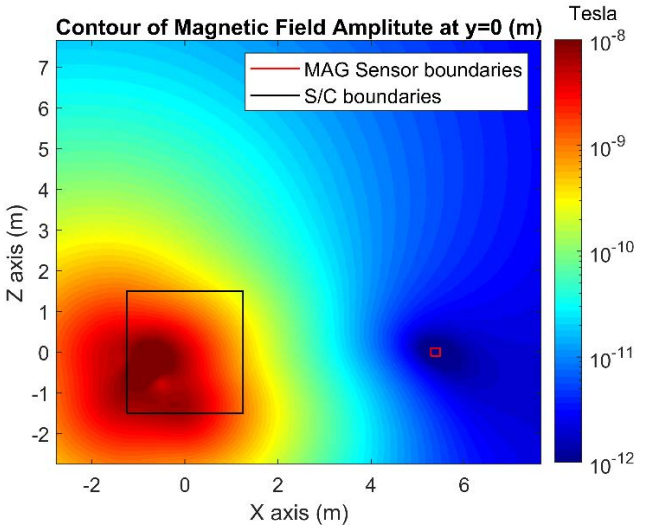

FIGURE 12. Magnetic field amplitude across the XZ plane at the center of the magnetic sensor ($5.386\ m$,$0\ m$,$0\ m$).

the spacecraft so there exist large field values due to high proximity to the sources (DUTs). So, the sensor being in a lower amplitude area is generally expected. However, as is clearly depicted in these two figures, as well as Fig. 9 which depicts a YZ plane away from the sources, the sensor is at all three slices at the area of minimum field. This is also evident from Fig, 10, which depicts the variation of electric field amplitude on the length of boom (but not limited to).

Starting at (1.25m, 0m, 1.5m), i.e., the point of the spacecraft where the boom is attached, and travelling towards the sensors on the boom line the electric field amplitude is minimized at the sensor location, dropping almost two orders of magnitude compared to nearby locations on the boom. Further on the boom the field amplitude increases again, clearly depicting the cleanliness achieved at the sensor.

At this point, authors must clarify that the boom line as referred to by Figs. 10 and 14 is depicted in Fig. 6 (blue line) and it lies on the XZ plane ($y = 0$ m).

Figures 11-13 depict contours of the magnetic field amplitude at the center of the magnetic sensor (5.386 m, 0 m, 0 m). The algorithm manages with the same arrangement of the DUTs to form the magnetic field in 3D space in such a way that the magnetic sensor is found at the same time at the location of minimum magnetic field for each plane. Identically, Figures 11-12 are 3D slices of the magnetic field amplitude which cut through the spacecraft so also in this case there exist large field values due to high proximity to the sources (DUTs).

However, as Fig. 13 depicts (YZ plane at x=5.386 m), the sensor is at the area of minimum field in this as well

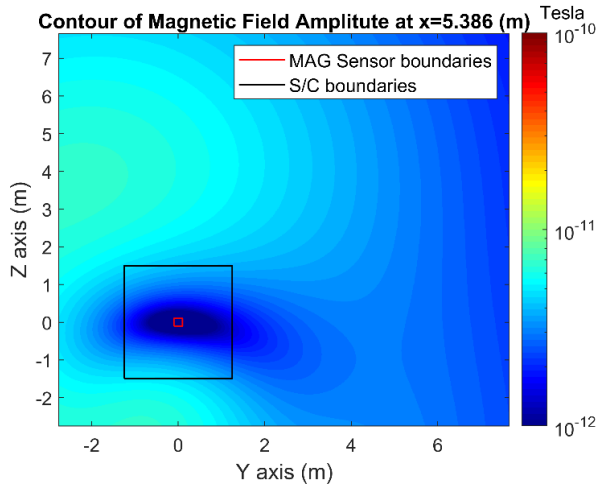

FIGURE 13. Magnetic field amplitude across the YZ plane at the center of the magnetic sensor ($5.386\ m$,$0\ m$,$0\ m$).

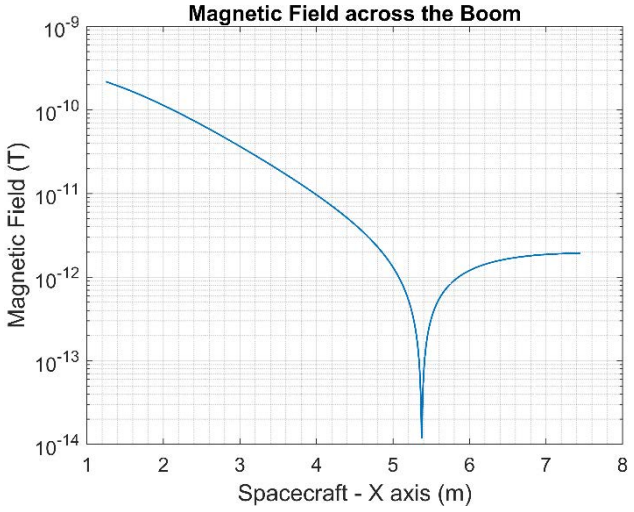

FIGURE 14. Magnetic Field amplitude on the boom. Minimum is at the magnetic sensor.

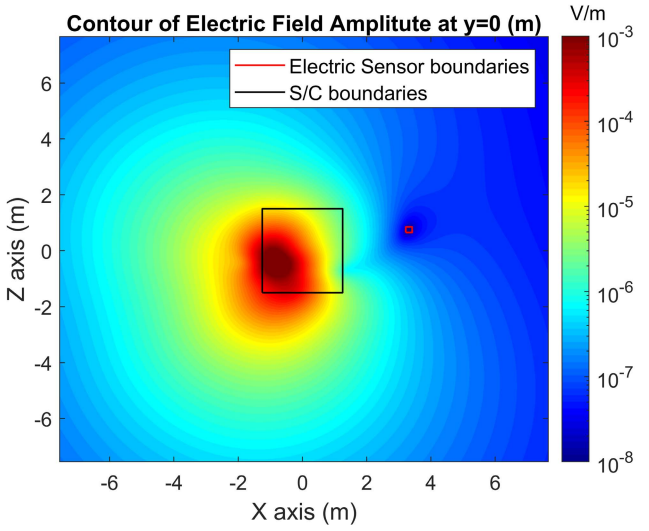

FIGURE 15. Electric field amplitude across the XZ plane at the center of the electric sensor ($3.318\ \ m$,$0\ m$,$0.75\ m$).

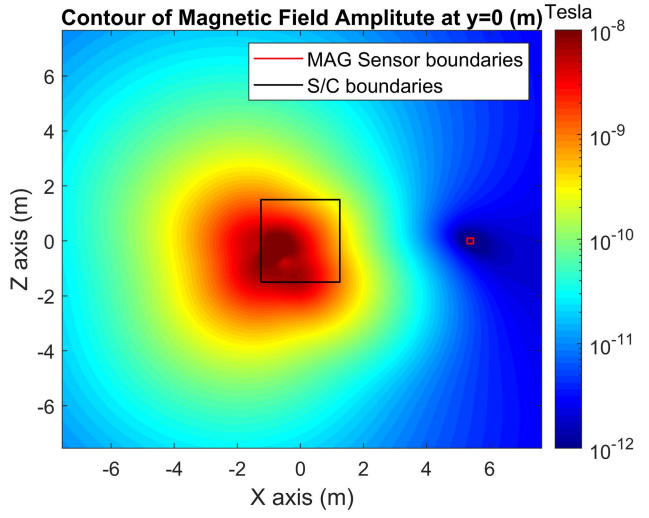

FIGURE 16. Magnetic field amplitude across the XZ plane at the center of the magnetic sensor ($5.386\ m$,$0\ m$,$0\ m$).

as the other two planes (XY and XZ planes). The same conclusion can be reached from Fig, 14, which depicts the variation of magnetic field amplitude on the length of boom. Across the boom line, travelling from the spacecraft towards the sensors the magnetic field amplitude is minimized at the sensor location, dropping almost two orders of magnitude compared to nearby locations on the boom. In this location, the magnetic sensor registers the least magnetic field possible among all neighboring areas due to the units of the spacecraft.

To further demonstrate the minimization of the electric and magnetic field achieved with the described algorithm, the field amplitude is calculated around the spacecraft across a larger area (approx. 15 m × 15 m × 15 m). Figures 15-16 depict the XZ plane cuts of the electric and magnetic field amplitudes respectively. It is evident that there is no other location in the area of study that presents a lower or a similarly low field level in either of the fields. This demonstrates the methodology's capacity to present unit arrangements that achieve joint electric and magnetic cleanliness, at levels suitable at least for early design considerations in missions.

IV. CONCLUSION

In this paper, the proposed methodology employs heuristics to derive an optimal arrangement (position and orientation) of DUTs, with known - predefined at unit level measurement campaign - magnetic and electric moments, in a spacecraft. The scope of this study is the joint minimization of the total magnetic and electric field amplitudes at separate sensor location. Authors showcase that given the electric and magnetic models of the units, the fields can be minimized at pre-selected and distinct areas of interest, where the sensors need to be placed. The solution manages to reduce the

fields by approximately two orders at the sensor locations. Limitations and restrictions on the unit placement can be easily implemented. Moreover, the methodology can be easily combined with active strategies to further enhance the results. Future work can include the expansion of the methodology to account also for the cable and harness emissions as to yield a harness path suitable for the joint cleanliness purpose. Also, the spacecraft walls shielding effects should also be included in the algorithm in order to ensure more accurate results and increase the robustness of the methodology. This will enable the use of the methodology to produce automatically an excellent starting point for the realization of an electromagnetically clean platform. Moreover, a measurement campaign at system level and the application of the proposed methodology to an actual spacecraft environment would be the ultimate validation test.

REFERENCES

[1] M. Pudney, S. King, T. Horbury, M. Maksimovic, C. J. Owen, and P. Laget, "Solar orbiter strategies for EMC control and verification," in *Proc. ESA Workshop Aerosp. EMC (Aerospace EMC)*, May 2019, pp. 1–6, doi: 10.23919/AeroEMC.2019.8788930.

[2] R. Leach, "Failures and anomalies attributed to electromagnetic interference," in *Proc. Space Programs Technol. Conf.*, Sep. 1995, p. 3654, doi: 10.2514/6.1995-3654.

[3] A. Junge and F. Marliani, "Prediction of DC magnetic fields for magnetic cleanliness on spacecraft," in *Proc. IEEE Int. Symp. Electromagn. Compat.*, Aug. 2011, pp. 834–839, doi: 10.1109/ISEMC.2011.6038424.

[4] F. S. de Adana, M. F. Catedra, J. M. Gomez, and R. Mittra, "Effective technique for system level prediction of the radiated emissions of electronic devices and cables inside satellites from unit level measurements," in *Proc. IEEE Int. Symp. Electromagn. Compat.*, Jul. 2007, pp. 1–5, doi: 10.1109/ISEMC.2007.185.

[5] F. S. de Adana, M. F. CÁtedra, J. M. GÓmez, R. Mittra, J. B. Renuncio, F. GutiÉrrez, and M. A. Prieto, "An effective technique for system-level prediction of the radiated emissions of unknown sources inside low-Q cavities using unit-level measurements," *IEEE Trans. Electromagn. Compat.*, vol. 51, no. 2, pp. 181–191, May 2009, doi: 10.1109/TEMC.2008.2010498.

[6] M. de Soria-Santacruz, M. Soriano, O. Quintero, F. Wong, S. Hart, M. Kokorowski, B. Bone, B. Solish, D. Trofimov, E. Bradford, C. Raymond, P. Narvaez, C. Keys, P. Lord, J. Ream, R. Oran, B. P. Weiss, C. Russell, K. Ascrizzi, and L. Elkins-Tanton, "An approach to magnetic cleanliness for the psyche mission," in *Proc. IEEE Aerosp. Conf.*, Mar. 2020, pp. 1–15, doi: 10.1109/AERO47225.2020.9172801.

[7] M. Boghosian, P. Narvaez, and R. Herman, "Magnetic testing, and modeling, simulation and analysis for space applications," in *Proc. IEEE Int. Symp. Electromagn. Compat.*, Aug. 2013, pp. 265–270, doi: 10.1109/ISEMC.2013.6670421.

[8] M. Pudney, S. King, C. Trenkel, F. Liebold, S. Strandmoe, P. Meyer, and M. Ehinger, "Advances in reaction wheel design for magnetic cleanliness," in *Proc. ESA Workshop Aerosp. EMC (Aerospace EMC)*, May 2019, pp. 1–6, doi: 10.23919/AeroEMC.2019.8788960.

[9] K. Dang, P. Narvaez, J. Berman, K. Pham, and A. Curiel, "Magnetic shielding concepts for reaction wheel assembly on NASA Europa clipper spacecraft," in *Proc. IEEE Int. Symp. Electromagn. Compat. Signal/Power Integrity (EMCSI)*, Jul. 2020, pp. 305–311, doi: 10.1109/EMCSI38923.2020.9191616.

[10] A. Nicolai, S. Stoltz, O. Hillenmaier, J. Ludwig, C. Strauch, D. Grivon, L. Rossini, E. Onillon, T. Hellwig, and S. Scheiding, "Towards a magnetically clean reaction wheel with active magnetic field mitigation," in *Proc. ESA Workshop Aerosp. EMC (Aerospace EMC)*, May 2019, pp. 1–6, doi: 10.23919/AeroEMC.2019.8788947.

[11] A. Nicolai, S. Stoltz, L. Hafemeister, S. Scheiding, O. Hillenmaier, and C. Strauch, "The magnetically clean reaction wheel: Results and performance," in *Proc. ESA Workshop Aerosp. EMC (Aerospace EMC)*, May 2022, pp. 1–7, doi: 10.23919/AerospaceEMC54301.2022.9828554.

[12] A. Lassakeur and C. Underwood, "Magnetic cleanliness program on CubeSats for improved attitude stability," in *Proc. 9th Int. Conf. Recent Adv. Space Technol. (RAST)*, Jun. 2019, pp. , doi: 10.1109/RAST.2019.8767816.

[13] R. Kallenbach, T. Behnke, S. Engelke, K. Bubeck, and R. Henkelmann, "AC and transient magnetic emissions of the juice Ganymede laser altimeter," in *Proc. ESA Workshop Aerosp. EMC (Aerospace EMC)*, May 2022, pp. 123–129, doi: 10.23919/AerospaceEMC54301.2022.9828840.

[14] T. Stern and S. DeLapp, "Techniques for magnetic cleanliness on spacecraft solar arrays," in *Proc. 2nd Int. Energy Convers. Eng. Conf.*, Aug. 2004, p. 5581, doi: 10.2514/6.2004-5581.

[15] V. A. Davis et al., "Surface-charging analysis of the radiation belt storm probe and magnetospheric multi scale spacecraft," Tech. Rep., 2012, doi: 10.1109/TPS.2011.2178615.

[16] G. I. Koutantos, C. D. Nikolopoulos, A. T. Baklezos, and C. N. Capsalis, "Proper equipment ordinance for achieving EM cleanliness in space missions: The case of ELF electric sources," *IEEE Trans. Electromagn. Compat.*, vol. 62, no. 5, pp. 1686–1692, Oct. 2020, doi: 10.1109/TEMC.2019.2937379.

[17] C. D. Nikolopoulos, A. T. Baklezos, and C. N. Capsalis, "On achieving spacecraft level magnetic cleanliness with proper equipment ordinance of DC and ELF magnetic sources," *IEEE Trans. Electromagn. Compat.*, vol. 62, no. 6, pp. 2714–2724, Dec. 2020, doi: 10.1109/TEMC.2020.2992682.

[18] A. T. Baklezos, C. D. Nikolopoulos, S. T. Spantideas, E. G. Chatzineofytou, M. Nicoletto, I. Marziali, D. Boschetti, and C. N. Capsalis, "Steady state emissions modeling of low frequency magnetic and electric fields generated by GOCE CDMU," in *Proc. ESA Workshop Aerosp. EMC (Aerospace EMC)*, May 2019, pp. 1–5, doi: 10.23919/AeroEMC.2019.8788927.

[19] H. H. Park, H. Jin, T. Y. Kim, K. H. Kim, H. J. Lee, J. H. Shin, Y. H. Jang, and W. H. Jo, "Analysis of the KPLO magnetic cleanliness for the KMAG instrument," *Adv. Space Res.*, vol. 69, no. 2, pp. 1198–1204, Jan. 2022, doi: 10.1016/j.asr.2021.11.015.

[20] A. S. K. Habila and W. H. Steyn, "In-orbit estimation of the slow varying residual magnetic moment and magnetic moment induced by the solar cells on CubeSat satellites," in *Proc. Int. Conf. Comput., Control, Electr., Electron. Eng. (ICCCEEE)*, Feb. 2021, pp. 1–6, doi: 10.1109/ICCCEEE49695.2021.9429618.

[21] M. A. Pudney, G. Kapfunde, and L. Trougnou, "Induced magnetic field due to reaction wheel shielding," in *Proc. ESA Workshop Aerosp. EMC (Aerospace EMC)*, May 2016, pp. 1–6, doi: 10.1109/AeroEMC.2016.7504601.

[22] R. Storn and K. Price, "Differential evolution—A simple and efficient heuristic for global optimization over continuous spaces," *J. Global Optim.*, vol. 11, no. 4, pp. 341–359, 1997, doi: 10.1023/A:1008202821328.

NIKOLAOS FRAGIADAKIS received the B.S. degree from the University of Ioannina (UOA), in 1981, and the M.Sc. degree in physics and telecom engineering from the National and Kapodistrian University of Athens (UOA), in 1983. He is currently pursuing the Ph.D. degree with the Department of Electronic Engineering, Hellenic Mediterranean University (HMU).

He is also an Application Lecturer of automatic control electronic systems with the Department of Electronic Engineering, HMU. His main research interests include electromagnetic compatibility, inverse scattering problems, electromagnetic field modeling for space applications, and EM cleanliness.

ANARGYROS T. BAKLEZOS was born in Lamia, Greece, in 1981. He received the B.S. and M.Sc. degrees in physics and telecom engineering from the National and Kapodistrian University of Athens (UOA), in 2008 and 2014, respectively, and the Ph.D. degree from the National Technical University of Athens (NTUA), in 2020.

He is currently an Adjunct Lecturer at the Department of Electronic Engineering, Hellenic Mediterranean University (HMU), and a Researcher at the School of Electrical and Computer Engineering, NTUA. His main research interests include electromagnetic compatibility, inverse scattering problems, electromagnetic field modeling for space applications, EM cleanliness, and antenna design for radiometry applications.

THEODOROS N. KAPETANAKIS was born in Chania, Crete, Greece, in 1984. He received the B.S. degree in electronic engineering and the M.Sc. degree in telecommunication and automation systems from Hellenic Mediterranean University (HMU), and the Ph.D. degree from the Department of Informatics and Telecommunications, University of Peloponnese (UoP).

He is currently an Adjunct Lecturer at the Department of Electronic Engineering, School of Engineering, HMU, and a Postdoctoral Researcher at the Telecommunications and Electromagnetic Applications Laboratory (TELEMA Lab). His research interests include applications of artificial intelligence and machine learning in propagation, radiation and scattering of electromagnetic waves, computational electromagnetics, bio-electromagnetics, and wearable microwave applications.

IOANNIS O. VARDIAMBASIS received the Diploma degree in electrical engineering and the Ph.D. degree in electrical and computer engineering from the National Technical University of Athens (NTUA), Greece.

He is currently an Associate Professor of microwave communications at the Department of Electronic Engineering, Hellenic Mediterranean University (HMU). He has served in several administrative positions at HMU, for many years, such as the Dean and the Vice-Dean of the Faculty of Applied Sciences; the Head of the Department of Electronic Engineering; and the Director of the Division of Telecommunications, the Telecommunications and Electromagnetic Applications Laboratory, and the Master's Program in telecommunication and automation systems. He has published more than 90 scientific papers in referred journals and international conference proceedings. He has participated as a research engineer in more than 30 Greek and EU-funded research and technological development ICT projects, being scientific coordinator in more than ten of them. His research interests include antennas, waveguides, microwave technology and applications, electromagnetic wave propagation, radiation and scattering, biological effects of electromagnetic fields, wearable technology, boundary value problems, wireless communications, sensors networks, neural networks, and artificial intelligence.

CHRISTOS D. NIKOLOPOULOS was born in Athens, Greece, in 1981. He received the B.S. and M.Sc. degrees in physics and telecom engineering from the National and Kapodistrian University of Athens (UOA), in 2006 and 2011, respectively, and the Ph.D. degree from the National Technical University of Athens (NTUA), in 2014.

He is an Assistant Professor at the Department of Electronic Engineering, Hellenic Mediterranean University (HMU). In addition to his long-standing affiliation as a Research Associate at the Wireless and Long-Distance Communication Laboratory, Department of Electrical and Computer Engineering, National Technical University of Athens. His main research interests include electromagnetic compatibility, inverse scattering, antenna design, and propagation. His recent research focuses on modeling and measuring techniques of electromagnetic emissions from space mission's equipment.